Highly Charged Ions for High-Resolution Soft X-ray Grating Monochromator Optimisation

Moritz Hoesch

DESY Photon Science, Deutsches Elektronen-Synchrotron, Notkestraße 85, 22607 Hamburg, Germany

E-mail: moritz.hoesch@desy.de

Jörn Seltmann

DESY Photon Science, Deutsches Elektronen-Synchrotron, Notkestraße 85, 22607 Hamburg, Germany

Florian Trinter

Institut für Kernphysik, Goethe-Universität Frankfurt am Main, Max-von-Laue-Straße 1, 60438 Frankfurt am Main, Germany
Molecular Physics, Fritz-Haber-Institut der Max-Planck-Gesellschaft, Faradayweg 4-6, 14195 Berlin, Germany

Steffen Kühn

Max-Planck-Institut für Kernphysik, Saupfercheckweg 1, 69117 Heidelberg, Germany

Moto Togawa

Max-Planck-Institut für Kernphysik, Saupfercheckweg 1, 69117 Heidelberg, Germany

René Steinbrügge

DESY Photon Science, Deutsches Elektronen-Synchrotron, Notkestraße 85, 22607 Hamburg, Germany

Sonja Bernitt

Helmholtz-Institut Jena, Fröbelstieg 3, 07743 Jena, Germany
GSI Helmholtzzentrum für Schwerionenforschung GmbH, Planckstraße 1, 64291 Darmstadt, Germany

José R. Crespo López-Urrutia

Max-Planck-Institut für Kernphysik, Saupfercheckweg 1, 69117 Heidelberg, Germany

Abstract. The energy-resolving performance of a synchrotron radiation monochromator can be characterised by measuring the fluorescence response of a gas in scans across characteristic absorption lines. Here, we describe a method using exceptionally narrow absorption features in the soft x-ray range. The features belong to helium-like ions and examples of the transition

1s $\rightarrow$ 2p in O^{6+} and Ne^{8+} are shown. We describe the instrument PolarX-EBIT and show typical data. A performance with ten times sharper effective feature width, when compared to neutral-gas absorption features, is demonstrated.

1. Introduction

Synchrotron radiation beamlines can deliver monochromatic VUV to soft x-ray beams with a resolving power up to $E/\Delta E = 10^5$ [1]. This resolution is achieved by a grating monochromator that, in the usually vertical dispersive plane, disperses the spread of photon energies and forms an image of the source on a precision slit unit, the exit slit [2, 3]. Beamlines with resolving power in this range are getting numerous, not only in the rather forgiving VUV range, but also in the soft x-rays, where the high resolving power is used for experiments approaching the scale of thermal excitations [4, 5, 6, 7, 8, 9]. Theoretically, even the creation of a monochromator with sub-meV resolution in the soft X-ray range is discussed [10].

The characterisation of such a monochromator is a challenge in itself. It is necessary, on one hand, to obtain a measured reference of the resolution profile, which can be used to convolve a theoretical prediction with the instrumental function to fully model an observed spectrum. On the other hand, the monochromator can be optimised by tuning parameters, and the measured resolution is the crucial control to find the optimal tune. Specifically, the focal length of the monochromator can be adjusted in almost all monochromator schemes, thus bringing the focus position of the dispersive plane upstream, downstream, or right on the exit-slit position. A high resolution is obtained only when this focus is correctly tuned. The experimental probe itself is often used to tune and measure the experimental resolution function [9]. This yields the relevant information, but requires tuning of both, the monochromator and the experiment. An impartial view of the monochromator performance in itself is thus desirable.

2. Monochromator and Beamline

The data shown in these proceedings were obtained on beamline P04 at the storage ring PETRA III [11]. This is a two-branch beamline with two separate monochromators, one of which can be served by a switching mirror unit. Rather than using the older branch that is mainly described in Ref. [11], where similar measurements have been made using the ion beam of PIPE [12, 13], here, we use the newer branch, which does not feature such a large installation.

The monochromator used here consists of a plane mirror and plane grating unit at 44 m from the source and an exit-slit unit at 64 m from the source. These two (mirror and grating) deflect the beam in the vertical plane, which is the dispersive plane of the monochromator. In addition, the beam passes over a horizontally deflecting plane switching mirror at 35 m and through a beam-defining aperture at 27.9 m. After the exit slit, the beam is focused into the instrument by a refocussing mirror unit to a beam waist of approximately 12×8 μm^2 (horizontal $\times$ vertical). The grating is of type variable line spacing with a central line density of 1200 lines/mm. This type of grating focusses the beam and the focal length is adjusted by the control parameter c_{ff} [2], which enters the computer-controlled adjustment of mirror and grating angles for the desired photon energy. The second tuning parameter is the exit-slit size. When all else is well tuned and focussed, the energy resolution increases linearly with decreasing slit size up to a limit given by the source size as demagnified by the monochromator and by optical imperfections.

3. PolarX-EBIT Electron-Beam Ion Trap

The instrument used here is the PolarX-EBIT Electron-Beam Ion Trap (EBIT) [14]. This instrument produces highly charged ions from a gas at pressures around 10^{-9} to 10^{-8} mbar by bombardment with an electron beam of energy up to 10 keV. The same focussed beam, along with

a magnetic field, traps the ions in a cloud of well below 100 μm diameter. A spectroscopic soft x-ray detector is used to detect fluorescence x-rays out of this cloud, tuned to select fluorescence from a specific atomic species, *e.g.*, oxygen or neon in the examples shown below. In the study shown here, we focus on ions with a simple helium-like electronic structure consisting of the nucleus and two electrons. These are $_8O^{6+}$ for oxygen and $_{10}Ne^{8+}$ for neon. In principle, any atomic species between $_3$Li and $_{26}$Fe or even heavier atoms can be brought into this configuration in the EBIT and both the fluorescence photon energy as well as the highest-energy absorption resonances are found at higher and higher photon energies with increasing charge of the nucleus. In this way, the method can be used at different, rather densely spaced, albeit discrete photon energies. Several sharp absorption resonances are found in the absorption spectra of these ions. Here, we focus on resonances that correspond to transitions 1s $\rightarrow$ 2p, labelled "w".

4. Results and Discussion

Fig. 1 shows the results from such an optimisation using the "w" resonance feature of oxygen, thus at a photon energy of approximately 574 eV. Panel (A) shows a spectrum before optimisation of the monochromator and using an enlarged exit-slit opening of 12 μm. Panel (B) shows the correponding spectrum after the optimisation. Here, the exit-slit size is 4 μm, below which no more significant improvement of the energy resolution can be expected and only the intensity of the beam is reduced proportional to the slit opening. Panel (C) summarises the progress of the optimisation. Here, we report the full width at half maximum (FWHM) as determined by Gaussian fits to the spectra. Through the increase of the resonance width on either side of the scan of c_{ff} it is clearly seen that the monochromator is defocussed for both, too small and too large c_{ff} and the focus is thus found, in this case, at $c_{ff} = 3.004$.

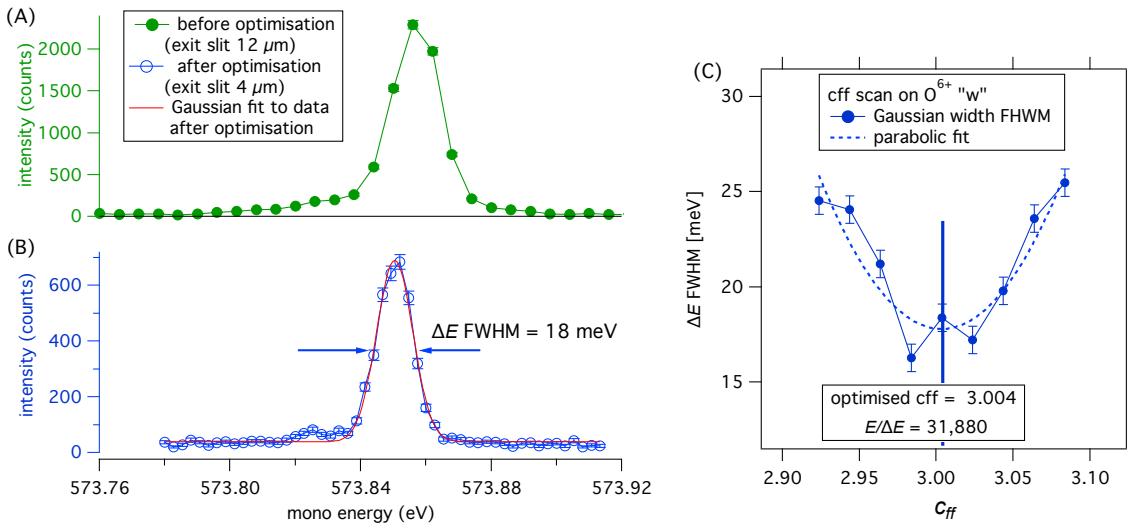

Figure 1. Optimisation results using the feature "w" (transition 1s $\rightarrow$ 2p) of O^{6+}. (A) Spectrum before optimisation of the monochromator and with a slightly enlarged exit-slit size for higher count rates. (B) Spectrum after optimisation. (C) Extracted width as a function of c_{ff} from spectra such as shown in (A) and (B). The minimum width, as determined by a parabolic fit, corresponds to the best focus.

As a cross check, we show a scan of the exit-slit opening in Fig. 2. The resolution clearly increases with decreasing slit opening, though not entirely linearly. A saturation at small slit

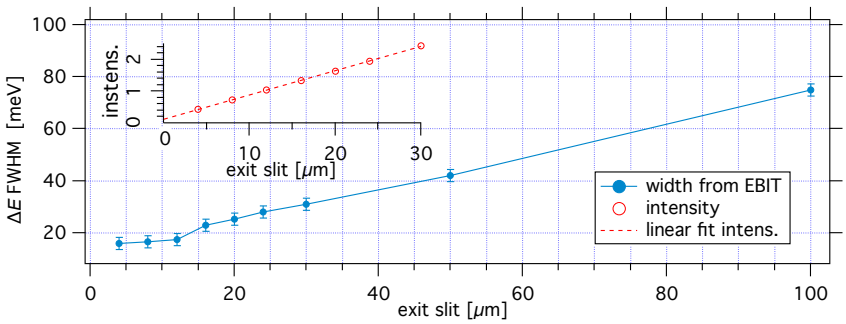

Figure 2. Extracted results of spectra of varying exit-slit size. The blue curve shows the extracted width FWHM and the inset shows the intensity of the spectra in arbitrary units.

openings is not discernible. The intensity, shown in the inset and extracted from the same spectra, shows a highly linear behaviour that also extrapolates zero at 0 μm exit-slit opening.

The analysis shown above focusses on the resonance width. This serves for the optimisation of the monochromator focal length, thus the formation of an image of the source on the exit-slit position. This image may, however, be distorted from other sources that affect not exclusively the width. Indeed the spectra shown in Fig. 1 clearly display a side bump of intensity on the lower energy side. This side bump is present in both spectra and appears as a pronounced small peak at the higher resolution of Fig. 1(B). The side bump is not a feature of the ion's absorption resonance, but rather it is allocated to monochromator imperfections and it was found that it can be influenced by settings of the primary beamline aperture at 27.9 m from the source. A different optimisation might thus tune the aperture opening and analyse the visibility of the side bump. The strength of the method is the observation of the full resolution function of the monochromator by making it visible through the well-defined and globally reproducible absorption profile.

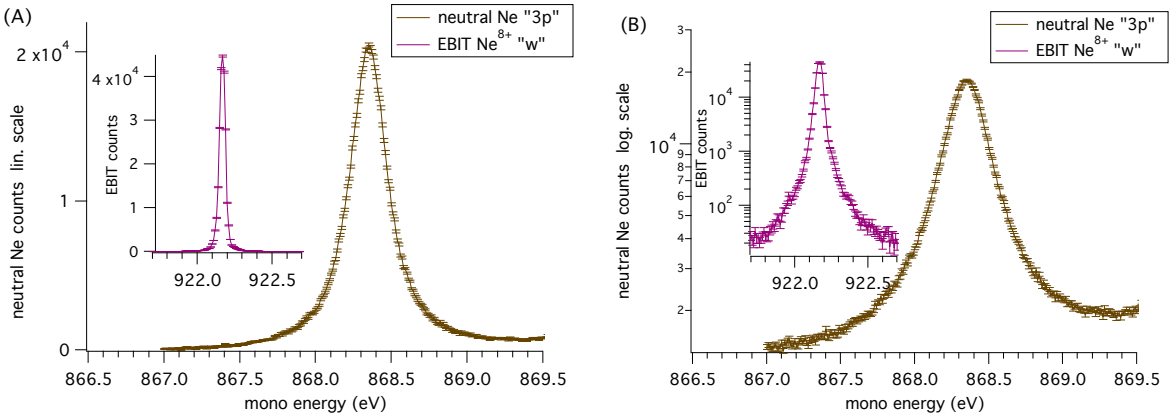

Figure 3. Absorption spectra of neutral Ne gas, measured with a separate detector, and of the "w" resonance of Ne^{8+}. (A) Linear scale of the intensity. (B) Logarithmic scale.

A set of spectra from Ne are shown in Fig. 3. The figure shows spectra of the "w" resonance of Ne^{8+} along with the well-known 1s $\rightarrow$ 3p resonance of neutral neon [5, 15]. The same information is shown on a linear scale in (A) and on a logarithmic scale in (B). Note that no calibration corrections have been applied to these data, thus the absolute photon energies indicated are

reliable to within a few eV only. The scales are, however, shown with identical scaling. The linear scale in Fig. 3(A) clearly demonstrates the approximately 10 times sharper feature size of the Ne^{8+} resonance when compared to neutral Ne.

We can now discuss the ultimate sensitivity of the method to the highest energy resolution. The data shown above demonstrate a feature width of $\Delta E = 18$ meV at $E = 574$ eV, thus a resolving power $E/\Delta E = 31,880$. The intrinsic ultimate resolution limit is given by the natural width of the resonance δE_{res}, which can be calculated as $\delta E_{O\text{“}w\text{”}} = 2.18$ meV [16]. Similar widths are found for the transition 1s $\rightarrow$ 2p in different ions. The observable resonance is, however, broadened by the motion of the ions, which is given by the ion-cloud temperature, and thus random in nature, the so-called Doppler broadening. This leads to a Gaussian effective resonance width of $\delta E_{Doppler} = E/c\sqrt{\ln 16}\sqrt{2k_BT/m}$, where E is the resonance energy, c is the speed of light, k_B is the Boltzmann constant, T is the temperature, and m is the ion mass [17]. At a temperature of estimated $T = 30,000$ K and for $E = 574$ eV and $m = 2.656{\cdot}10^{-26}$ kg for oxygen this corresponds to an effective width $\delta E = 17.8$ meV. The observed ΔE is a convolution of $\delta E_{Doppler}$ with the monochromator resolution function. Under the conditions of this experiment $\delta E_{Doppler}$ is the leading contribution to ΔE. Nevertheless, the observation of an increase of ΔE at either end of the focussing scan allows for a reliable determination of the correct best focus. The ultimate optimisation of the EBIT method can involve a next step of reducing the ion temperature, which can be done by adjusting the electron-beam parameters.

Summary

In summary, we have described how absorption resonances of type “w” in helium-like ions allow for the characterisation of the energy resolution of a soft x-ray monochromator. Two examples are specifically shown for O^{6+} and Ne^{8+} at $E = 574$ eV and $E = 922$ eV, respectively. The instrument required for generation of these ions and the detection of the signal is briefly discussed. The spectrum from Ne^{8+} is compared to neutral Ne, thus demonstrating the at least 10 times sharper feature size that depends only on the ion-cloud temperature and can thus be readily reproduced.

Acknowledgments

We thank Jens Viefhaus, Kai Bagschik, Stefan Schippers, and Alfred Müller for fruitful discussions. Financial support for PolarX-EBIT was provided by Bundesministerium für Bildung und Forschung (BMBF) through project 05K13SJ2.

References

[1] Weiss M, Follath R, Sawhney K, Senf F, Bahrdt J, Frentrup W, Gaupp A, Sasaki S, Scheer M, Mertins H C, Abramsohn D, Schäfers F, Kuch W and Mahler W 2001 *Nuclear Instruments and Methods in Physics Research Section A: Accelerators, Spectrometers, Detectors and Associated Equipment* **467-468** 449–452 ISSN 0168-9002 7th Int.Conf. on Synchrotron Radiation Instrumentation URL https://www.sciencedirect.com/science/article/pii/S0168900201003552

[2] Howells M R 2009 *X-Ray Data Booklet Section 4.3 Gratings and Monochromators* (Lawrence Berkeley National Laboratory University of California Berkeley, California 94720) URL http://xdb.lbl.gov/Section4/Sec_4-3.html

[3] Follath R and Senf F 1997 *Nuclear Instruments and Methods in Physics Research Section A: Accelerators, Spectrometers, Detectors and Associated Equipment* **390** 388–394 ISSN 0168-9002 URL https://www.sciencedirect.com/science/article/pii/S0168900297004014

[4] Strocov V N, Schmitt T, Flechsig U, Schmidt T, Imhof A, Chen Q, Raabe J, Betemps R, Zimoch D, Krempasky J, Wang X, Grioni M, Piazzalunga A and Patthey L 2010 *Journal of Synchrotron Radiation* **17** 631–643 URL http://scripts.iucr.org/cgi-bin/paper?S0909049510019862

[5] Yamamoto S, Senba Y, Tanaka T, Ohashi H, Hirono T, Kimura H, Fujisawa M, Miyawaki J, Harasawa A, Seike T, Takahashi S, Nariyama N, Matsushita T, Takeuchi M, Ohata T, Furukawa Y, Takeshita K, Goto S, Harada Y, Shin S, Kitamura H, Kakizaki A, Oshima M and Matsuda I 2014 *J Synchrotron Radiat* **21** 352 URL http://scripts.iucr.org/cgi-bin/paper?S1600577513034796

[6] Dvorak J, Jarrige I, Bisogni V, Coburn S and Leonhardt W 2016 *Review of Scientific Instruments* **87** 115109 URL https://aip.scitation.org/doi/10.1063/1.4964847

[7] Müller A, Lindroth E, Bari S, Borovik A, Hillenbrand P M, Holste K, Indelicato P, Kilcoyne A L D, Klumpp S, Martins M, Viefhaus J, Wilhelm P and Schippers S 2018 *Phys. Rev. A* **98**(3) 033416 URL https://link.aps.org/doi/10.1103/PhysRevA.98.033416

[8] Brookes N, Yakhou-Harris F, Kummer K, Fondacaro A, Cezar J, Betto D, Velez-Fort E, Amorese A, Ghiringhelli G, Braicovich L, Barrett R, Berruyer G, Cianciosi F, Eybert L, Marion P, van der Linden P and Zhang L 2018 *Nuclear Instruments and Methods in Physics Research Section A: Accelerators, Spectrometers, Detectors and Associated Equipment* **903** 175–192 ISSN 0168-9002 URL https://www.sciencedirect.com/science/article/pii/S0168900218308234

[9] Zhou K J, Walters A, Garcia-Fernandez M, Rice T, Hand M, Nag A, Li J, Agrestini S, Garland P, Wang H, Alcock S, Nistea I, Nutter B, Rubies N, Knap G, Gaughran M, Yuan F, Chang P, Emmins J and Howell G 2022 *Journal of Synchrotron Radiation* **29** 563–580 URL https://scripts.iucr.org/cgi-bin/paper?S1600577522000601

[10] Shvyd'ko Y 2020 *Journal of Synchrotron Radiation* **27** 1227–1234 URL https://scripts.iucr.org/cgi-bin/paper?S1600577520008292

[11] Viefhaus J, Scholz F, Deinert S, Glaser L, Ilchen M, Seltmann J, Walter P and Siewert F 2013 *Nuclear Instruments and Methods in Physics Research Section A: Accelerators, Spectrometers, Detectors and Associated Equipment* **710** 151–154 ISSN 0168-9002 the 4th international workshop on Metrology for X-ray Optics, Mirror Design, and Fabrication URL https://www.sciencedirect.com/science/article/pii/S0168900212012831

[12] Schippers S, Ricz S, Buhr T, Borovik A, Hellhund J, Holste K, Huber K, Schäfer H J, Schury D, Klumpp S, Mertens K, Martins M, Flesch R, Ulrich G, Rühl E, Jahnke T, Lower J, Metz D, Schmidt L P H, Schöffler M, Williams J B, Glaser L, Scholz F, Seltmann J, Viefhaus J, Dorn A, Wolf A, Ullrich J and Müller A 2014 *Journal of Physics B: Atomic, Molecular and Optical Physics* **47** 115602 URL https://iopscience.iop.org/article/10.1088/0953-4075/47/11/115602

[13] Schippers S, Buhr T, Borovik Jr A, Holste K, Perry-Sassmannshausen A, Mertens K, Reinwardt S, Martins M, Klumpp S, Schubert K, Bari S, Beerwerth R, Fritzsche S, Ricz S, Hellhund J and Müller A 2020 *X-Ray Spectrometry* **49** 11–20 URL https://analyticalsciencejournals.onlinelibrary.wiley.com/doi/abs/10.1002/xrs.3035

[14] Micke P, Kühn S, Buchauer L, Harries J R, Bücking T M, Blaum K, Cieluch A, Egl A, Hollain D, Kraemer S, Pfeifer T, Schmidt P O, Schüssler R X, Schweiger C, Stöhlker T, Sturm S, Wolf R N, Bernitt S and Crespo López-Urrutia J R 2018 *Review of Scientific Instruments* **89** 063109 URL https://aip.scitation.org/doi/10.1063/1.5026961

[15] Müller A, Bernhardt D, Borovik A, Buhr T, Hellhund J, Holste K, Kilcoyne A L D, Klumpp S, Martins M, Ricz S, Seltmann J, Viefhaus J and Schippers S 2017 *The Astrophysical Journal* **836** 166 URL https://iopscience.iop.org/article/10.3847/1538-4357/836/2/166

[16] Cann N M and Thakkar A J 1992 *Phys. Rev. A* **46**(9) 5397–5405 URL https://link.aps.org/doi/10.1103/PhysRevA.46.5397

[17] Tatum J 2022 Section 10.3 in URL http://orca.phys.uvic.ca/˜tatum/stellatm.html